Molinero-Fernández, Águeda *et al.* (2018) 'Magnetic Reduced Graphene Oxide/Nickel/Platinum Nanoparticles Micromotors for Mycotoxin Analysis', *Chemistry : a European journal*, 24(28), pp. 7172–7176.

doi:10.1002/chem.201706095

(Article begins on next page)

DOI: XXX

Analytical Methods |*Hot Paper*|

Magnetic Reduced Graphene Oxide/Nickel/Platinum Nanoparticles Micromotors for Mycotoxin Analysis

Águeda Molinero-Fernández,[a] Adrián Jodra,[a] María Moreno-Guzmán,[a] Miguel Ángel López,[a] and Alberto Escarpa*[a, b]

Abstract: Magnetic reduced graphene oxide/nickel/platinum nanoparticles (rGO/Ni/PtNPs) micromotors for mycotoxin analysis in food samples were developed for food-safety diagnosis. While the utilization of self-propelled micromotors in bioassays has led to a fundamentally new approach, mainly due to the greatly enhanced target–receptor contacts owing to their continuous movement around the sample and the associated mixing effect, herein the magnetic properties of rGO/Ni/PtNPs micromotors for mycotoxin analysis are additionally explored. The micromotor-based strategy for targeted mycotoxin biosensing focused on the accurate control of micromotor-based operations: 1) on-the-move capture of free aptamers by exploiting the adsorption (outer rGO layer) and catalytic (inner PtNPs layer) properties and 2) micromotor stopped flow in just 2 min by exploiting the magnetic properties (intermediate Ni layer). This strategy allowed fumonisin B1 determination with high sensitivity (limit of detection: 0.70 ng mL^{-1}) and excellent accuracy (error: 0.05% in certified reference material and quantitative recoveries of 104 ± 4% in beer) even in the presence of concurrent ochratoxin A (105–108 ± 8% in wines). These results confirm the developed approach as an innovative and reliable analytical tool for food-safety monitoring, and confirm the role of micromotors as a new paradigm in analytical chemistry.

Introduction

The motion of self-propelled micromotors in extremely small sample volumes for (bio)sensing purposes is one of the most exciting areas in contemporary analytical chemistry.[1–5] Nano/micromachines with different propulsion mechanisms such as ultrasonic, magnetic, and fuel propulsion have been reported.[3,6–9]

For micromotors chemically powered by bubble propulsion,[10,11] especially self-propelled motors based on hydrogen peroxide,[12,13] different aspects, such as their continuous movement around the sample and the associated mixing effect due to the generated microbubble tail,[14] have allowed the on-the-move target–receptor interaction to be greatly enhanced and the binding efficiency and sensitivity of these assays to be improved. This ability of nano/microscale motors to capture and transport specific target analytes in complex biological matrices have laid the foundations for novel biosensing methods[2,15] and applications.[1,3,6,16–18]

Micromotors have been constructed by different approaches including top-down photolithography, electron-beam evaporation, and stress-assisted rolling of functional nanomembranes on polymers.[10,11,19] However, template electrodeposition fabrication has proved to be a simpler and more economical processes for the preparation of bimetallic catalytic nanowires[12,20] and tubular micromotors.[21,22] Also, the incorporation of carbon nanomaterials in tubular micromotors has improved the propulsion performance because of the enhanced catalytic activity and efficient bubble evolution compared with smooth tubular micromotors.[23–25] Specifically, the exceptional surface properties of graphene have allowed the attachment of different receptors for toxin detection,[26,27] the capture and removal of nerve agents and heavy metals,[28] and excellent fluorescence-quenching ability based on an energy-transfer mechanism.[29–32]

On the other hand, mycotoxins are potent toxins that cause negative effects on animal and human health, and are now considered the most important chronic dietary risk factor, even more than food additives or pesticide residues.[33] Produced as secondary metabolites by various filamentous fungal species under different environmental conditions, their negative impact on public health has lead into the establishment of maximum permitted levels by the EU [e.g., 0.2 μg mL^{-1} for fumonisin B1 (FB1) and 0.002–0.01 μg mL^{-1} for ochratoxin A

[a] Á. Molinero-Fernández, Dr. A. Jodra, Dr. M. Moreno-Guzmán, Prof. M. Á. López, Prof. A. Escarpa
Department of Analytical Chemistry
Physical Chemistry and Chemical Engineering
University of Alcalá, Carretera Madrid-Barcelona, Km. 33,600
28871 Alcalá de Henares, Madrid (Spain)
Fax: (+34) 91-885-49-71
E-mail: alberto.escarpa@uah.es

[b] Prof. A. Escarpa
Chemical Research Institute "Andrés M. del Río" (IQAR)
University of Alcalá, Carretera Madrid-Barcelona
Km. 33,600, Alcalá de Henares, 28871 Madrid (Spain)

Supporting information and the ORCID identification number(s) for the author(s) of this article can be found under https://doi.org/10.1002/chem.201706095.

(OTA)].[34] Thus, the development of selective and sensitive analytical approaches is highly recommended.[35–38] Immunochemical methods and liquid chromatography coupled to tandem mass spectrometry (LC-MS/MS) have also been used for mycotoxin determination.[39] However, these methodologies are limited by their nonportability, need for trained personnel, and laborious and time-consuming nature, which make their implementation in several applications difficult.

Graphene-based micromotors for fast and simultaneous micotoxins determination in food samples have recently been reported by us.[15] The assay principle was based on the on-the-move fluorescence quenching of the free aptamer in the outer layer of unmodified rGO as sensing layer. To extend the applicability of the micromotors, in the present work, we used magnetic reduced graphene oxide/nickel/platinum nanoparticles (rGO/Ni/PtNPs) micromotors for biosensing of target mycotoxins in food samples. Herein, their adsorption, magnetic, and catalytic capabilities are reported.

Results and Discussion

Figure 1 illustrates the magnetic rGO/Ni/PtNPs micromotor-based strategy for mycotoxin biosensing focused on accurate control of micromotor-based operations: 1) on-the-move capture of free aptamers and consequently their fluorescence quenching by exploiting the adsorption (outer rGO layer) and catalytic (inner PtNPs layer) properties and 2) micromotor stopped flow in just 2 min by exploiting the magnetic properties (intermediate Ni layer).

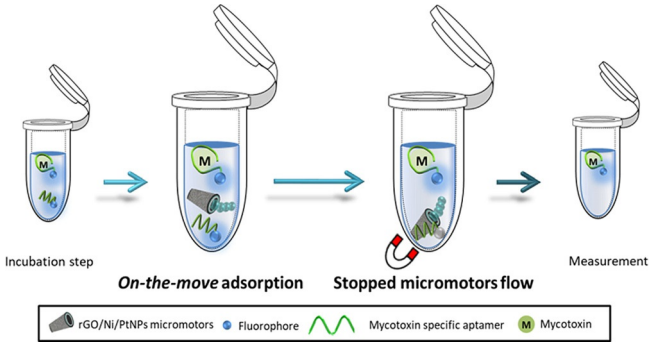

Figure 1. Magnetic rGO/Ni/PtNPs micromotors-based strategy for mycotoxins biosensing.

Adsorption of the free dye-labeled aptamers on outer rGO layer by π–π interactions between ring structures of the nucleotide bases and the hexagonal cells of graphene leads to their fluorescence quenching. Simultaneously, the high affinity of the specific aptamer to the mycotoxin causes formation of the complex, which decreases the exposure of nucleotides to the graphene micromotors and hence prevents aptamer adsorption by the outer rGO layer and allows their fluorescence.

The motion of the micromotors around the small sample volume, the mixing effect due to the localized fluid convection and vortex streams associated with the rapid movement of the micromotors, and the generated microbubble tail greatly improve the rGO–aptamer interaction. Thus, the required time for the micromotors to swim through the sample solution and reach the maximum number of free dye-labeled aptamers was just 2 min. This adsorption time is essential to assess the analytical signal based on the fluorescence of the mycotoxin–aptamer complex and was tremendously improved even in comparison with other reported values of up to 80 min for a solution containing a dispersion of graphene under normal stirring.[40] When a shaking system (Thermoshaker at 950 rpm) with identical sample volume was used for comparison, at least 30 min was needed for a quenching efficiency of about 85%. This shows that the micromotors action greatly improves the rGO–aptamer interaction, even on board of magnetic micromotors.

Characterization of rGO/Ni/PtNPs micromotors was also carried out by SEM and energy-dispersive X-ray spectroscopy (EDX) analysis. SEM-EDX images revealed a tubular shape (Figure 2A) and a composition (Figure 2B) of carbon, nickel and platinum corresponding to the outer (rGO, adsorption), intermediate (Ni, magnetic), and inner (PtNPs, catalytic) layers, respectively. These results confirmed successful micromotor fabrication. Figure 2C shows the fluorescence mapping of fluorophore-labeled aptamer specific for FB1 and FB1 mycotoxin. Excitation and emission wavelengths of $\lambda_{ex}^{FB} = 470$ nm and $\lambda_{em}^{FB} = 520$ nm were chosen for FB1 detection.

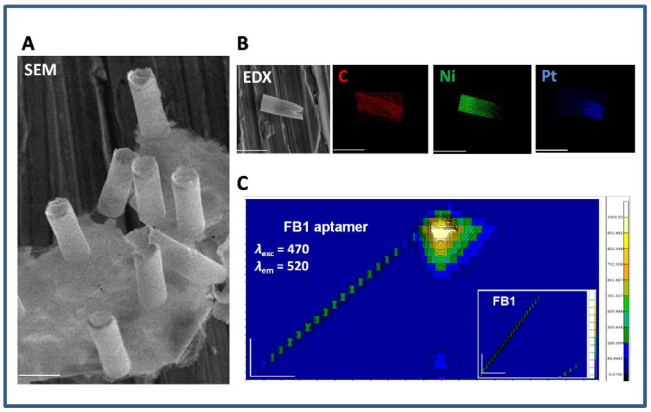

Figure 2. A) SEM analysis. Scale bar: 10 μm. B) EDX analysis. Scale bar: 10 μm. C) 3D fluorescence spectra of fluorophore-labeled aptamer and FB1 (300–540 nm for excitation and 300–700 nm for emission). Scale bar: 50 nm.

Then, the amount of micromotors and the concentration of dye-labeled aptamers were carefully optimized. For a fixed aptamer concentration of 5 μM, which produces enough fluorescence intensity, the influence of the amount of micromotors on the aptamer adsorption and hence the fluorescence quenching of the free aptamer is shown in Figure 3A. In the absence of the mycotoxin (orange bars), with increasing number of micromotors, fluorescence quenching also increases, and the optimum number of micromotors to obtain the maximum quenching effect is around 4500. Interestingly, when a 1 $\mu g\,mL^{-1}$ concentration of FB1 was added to the solution (blue bars), the maximum fluorescence emission remained con-

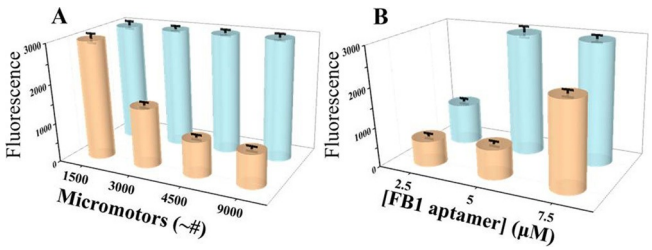

Figure 3. Optimization of the number of rGO/Ni/PtNPs micromotors (aptamer concentration: 5 μM; A) and aptamer concentration (number of micromotors: ≈4500; B). Blue and orange colors represent the presence of 1 μg mL^{-1} mycotoxin and absence of mycotoxin, respectively.

stant, and it demonstrated the negligible quenching effect of the FB1–aptamer complex.

The influence of aptamer concentration was also tested. As shown in Figure 3B, 5 μM was the optimum concentration, since lower aptamer concentration produces a weaker fluorescence signal, even in the presence of the mycotoxin. This indicates that the signal is limited by the aptamer concentration and not by the quenching effect. Fluorescence increased in the absence of the mycotoxin for higher aptamer concentrations, as a consequence of an excess of the dye-labeled aptamer over the micromotor amount avoiding total quenching.

Table 1 lists the analytical characteristics of the rGO/Ni/PtNPs micromotors-based method for FB1 mycotoxin determination. Excellent linearity ($r = 0.990$) as well as limits of detection (LOD = 0.7 ng mL^{-1}, $S/N = 3$ criterion) and quantification (LOQ = 5 ng mL^{-1}, $S/N = 10$ criterion) were obtained for the FB1 assay.

Table 1. Analytical characteristics of the rGO/Ni/PtNPs micromotors-based approach.

Mycotoxin	Linear range [μg mL^{-1}]	Equation	r	LOD [μg mL^{-1}]
FB1	0.005–1	$y = 903.9x + 3093.3$	0.990	0.0007
OTA	0.01–10	$y = 104.3x + 682.8$	0.990	0.004

These values, which are well below the legal requirements of the EU (0.2 μg mL^{-1} for FB1),[35] reveal the suitability of this novel strategy for FB1 assessment in foodstuffs. Evaluation of precision at two mycotoxin concentrations (0.01 and 1 μg mL^{-1}) yielded relative standard deviations (RSD) of 7 and 5%, respectively ($n = 5$, independent micromotor batches).

Since OTA is a common concurrent mycotoxin with high significance, its determination by this approach was also explored. By using appropriate excitation and emission wavelengths for both mycotoxins ($\lambda_{ex}^{FB} = 470$ nm, $\lambda_{em}^{FB} = 520$ nm; $\lambda_{ex}^{OTA} = 585$ nm; $\lambda_{em}^{OTA} = 602$ nm), good selectivity (cross-reactivity of 5 and 10% for FB1 and OTA determination, respectively) was obtained. The OTA calibration data are also listed in Table 1.

Table 2 lists the results of FB1 determination in food samples. Outstanding accuracy was obtained when certified reference material (CRM) was analyzed (error < 0.05%). Also, quantitative and reproducible recoveries (104 ± 4%) obtained during the analysis of beer samples revealed its suitability for their analysis. Excellent quantitative and reproducible recoveries of 108 ± 8% were also obtained for OTA assessment in wine samples (even in red wines, which are quite difficult), which demonstrated the accuracy in the simultaneous determination of concurrent mycotoxins and revealed the analytical potency of the approach.

Table 2. Analysis of food samples.

Mycotoxin	Sample	Reference value [μg mL^{-1}]	Found value [μg mL^{-1}]	Error/recovery [%]
FB1	CRM	0.23 ± 0.05	0.23 ± 0.02	0.05
	beer	0.20	0.21 ± 0.01	104 ± 4
OTA	white wine	0.20	0.22 ± 0.02	108 ± 8
	red wine	0.20	0.21 ± 0.02	105 ± 8

Indeed, this strategy exploits not only the adsorption properties of outer rGO layer, but also the magnetic properties derived from the Ni layer, which allowed accurate control of micromotor operations. Because of the adsorption of the aptamers on the outer rGO layer, the rGO/Ni/PtNPs micromotors played a unique role, since they acted as mobile micro clean-up/sorbent systems. Indeed, they allowed very easy removal of the clear supernatants with the aid of a magnet, and thus open novel avenues for analytical operations involving heterogeneous phases. Therefore, this approach is a clear alternative to magnetic particles with the inherent advantages of micromotor self-mixing in ultrasmall sample volumes (< 10 μL) and functionalization opportunities for on-the-move biosensing.

Figure 4 and Video S1 (Supporting Information) show the rGO/Ni/PtNPs micromotors swimming in the analyzed samples (PBS-T buffer, CRM, beer, white wine, and red wine) with speeds of 120 ± 30, 90 ± 20, 110 ± 30, 90 ± 10, and 80 ± 20 μm s^{-1}, respectively (at 1% v/v added H_2O_2). As expected,

Figure 4. rGO/Ni/PtNPs micromotors swimming in different samples (1% H_2O_2 added). Scale bar: 5 μm.

the speed of magnetic rGO/Ni/PtNPs micromotors was decreased in comparison with nonmagnetic ones (rGO/PtNPs) with speeds of 360 ± 60, 260 ± 50, 320 ± 90, and 280 ± 90 μm s^{-1}, for PBS-T buffer, CRM, and beer, respectively,[15] due to the incorporation of Ni. However, this did not hamper obtaining excellent analytical performance during the analysis of food samples, as is demonstrated in Table 2. Furthermore, the fluorescent mycotoxin–aptamer complex and the quenching effect of the free aptamer by micromotors gave identical values in both food samples and standards and thus revealed the adsorption capacity of rGO in real environments due to efficient micromotor navigation in food samples.

Conclusion

Magnetic rGO/Ni/PtNPs micromotors are a smart and powerful analytical tool for mycotoxin analysis in foods. Exploiting adsorption, magnetic, and catalytic properties allowed accurate control of micromotor operations. The on-the-move adsorption of free aptamer was performed in just 2 min, a dramatic improvement compared to the reported literature, with excellent sensitivity, selectivity, and accuracy in concurrent FB1 and OTA mycotoxin analysis in food samples. These results allow an exciting future for the novel applications of micromotors in unexplored fields such as food safety diagnosis to be envisioned and confirm the role of micromotors as a new paradigm in analytical chemistry.

Experimental Section

Reagents and materials

Fluorescein amidine (FAM) labeled at the 5′-end aptamer, specific for FB1 (FAM-5′-ATA CCA GCT TAT TCA ATT AAT CGC ATT ACC TTA TAC CAG CTT ATT CAA TTA CGT CTG CAC ATA CCA GCT TAT TCA ATT AGA TAG TAA GTG CAA TCT-3′) and the ROX-OTA aptamer, specific for OTA and labeled at the 5′ end with rhodamine X (ROX) (ROX-5′-GGG AGG ACG AAG CGG AAC CGG GTG TGG GTG CCT TGA TCC AGG GAG TCT CAG AAG ACA CGC CCG ACA-3′), were synthetized by Microsynth (The Swiss DNA company, Switzerland). Graphene oxide (GO) was purchased from Sigma-Aldrich (2 mg mL^{-1} dispersion in H_2O, ref: 763705). FB1, OTA, hydrogen peroxide, sodium dodecyl sulfate (SDS), H_2SO_4, Na_2SO_4, H_2PtCl_6, boric acid, propan-2-ol, and ethanol were purchased from Sigma-Aldrich. Hydrogen peroxide solution (1% v/v) was used as the chemical fuel, and SDS solution (1% v/v) as the surfactant in all propulsion experiments. Aptamers were reconstituted in 10 mM Tris-HCl buffer (pH 7.5, 100 μM) and stored at +4 °C until use. Stock dilution of FB1 (50 μg mL^{-1}) was done in ethanol. Phosphate-buffered saline (100 mM pH 7.5) was prepared with Milli-Q water and 0.01% of Tween (PBS-T) and used for dilution of FAM–aptamer, ROX–aptamer, and mycotoxins. All chemicals used were analytical-grade reagents, and deionized water was obtained from a Millipore Milli-Q purification system (18.2 MΩ cm at 25 °C).

Maize fumonisin CRM ([FB1] = 2.0 ± 0.4 mg kg^{-1}; [FB2] = 0.5 ± 0.2 mg kg^{-1}; [FB3] = 0.2 ± 0.1 mg kg^{-1}) was purchased from Pribolabs (Singapore). According to the instructions recommended by the supplier, 1 g sample aliquots were extracted with 4 mL of acetonitrile/PBS (50:50, v/v) under refrigeration conditions by tip sonication (VCX130, Sonics, Newtown, USA) for 20 min (5 min/cycle) at 117 W. After centrifugation at 4000 rpm for 10 min, the supernatant was separated. Beer (Draught Guinness, Dublin, Ireland) was first degasified for 20 min in an ultrasonic bath and immediately spiked with different FB1 concentrations. White and red wines (Cataluña, Spain) were spiked with different concentrations of OTA.

Apparatus

Template-assisted electrochemical deposition of micromotors was carried out with a μ-Autolab Type III electrochemical station (Eco Chemie, Utrecht, Holland). SEM images were obtained with a JEOL JSM 6335F instrument at an acceleration voltage of 22 kV. EDX mapping was performed with an EDX detector attached to the SEM instrument. A Dilor XY Raman spectrometer, equipped with two types of detectors (one matrix-type and one photomultiplier) with measurement in the sample and by microscope, was used. It is equipped with two alternative sources: Kr^+ Coherent Innova 70-K laser and Ar^+ Coherent Innova 90C laser. An inverted optical microscope (Nikon Eclipse 80i upright microscope), coupled with different objectives (10×, 20×, and 40×), a B2-A fluorescence filter (λ_{ex} = 470 nm, λ_{em} = 520 nm) for FAM, G-2A fluorescence filter (λ_{ex} = 585 nm, λ_{em} = 602 nm) for ROX, a Hamamatsu C11440 digital camera, and NIS Elements AR 3.2 software, was used for capturing images and movies at a rate of 30 frames per second. A PerkinElmer LS-50B luminescence spectrophotometer equipped with a Xe flash lamp and quartz cuvettes of 1 cm path length thermostated with a Thermomix BU bath for fluorescence measurements was also used. The excitation and emission slit widths were 5 nm and the scan speed was 1000 nm min^{-1}. Data acquisition and analysis were carried out with the PerkinElmer Flwin Lab software. The speed of the micromotors was tracked with an NIS Elements tracking module. The fluorescence signal produced by the hybridization process between the dye–aptamer and the target mycotoxin was estimated by analyzing the corresponding time-lapse images with the Gwyddion software. Aptamer–mycotoxin incubation steps were performed in a Thermoshaker TS-100C from Biosan (Latvia).

Methods

Electrosynthesis of graphene micromotors: The rGO micromotors were prepared by electrochemical reduction of graphene oxide into 5 μm-diameter conical pores of a polycarbonate membrane (Catalog No. 7060-2513, Whatman, Maidstone, UK). The branched side of the membrane was treated with a sputtered thin gold film to perform as a working electrode. The membrane was assembled in a Teflon plating cell with aluminum foil serving as an electrical contact to the working electrode for the subsequent electrodeposition. GO (0.5 mg mL^{-1}) was first dispersed in a solution containing 0.1 M H_2SO_4 and 0.5 M Na_2SO_4 in an ultrasonic bath for 15 min. The electrochemical reduction of GO was carried out by cyclic voltammetry (+0.3 to −1.5 V vs. Ag/AgCl (3 M KCl) at 50 mV s^{-1} for five cycles; n = 5) by using a Pt wire as counter electrode. A magnetic layer of Ni was incorporated in the micromotor structure for efficient magnetic control of the micromotor. The nickel tube layer was plated inside the reduced carbon layer by galvanostatic method. First, ten pulses of −20 mA were applied for 0.1 s to generate nucleation spots. Then, a constant current of −6 mA was applied for 300 s to grow the nickel layer.[41] Subsequently, a platinum layer was plated inside the rGO tube. The inner PtNPs layer was deposited by amperometry at −0.4 V for 750 s from an aqueous solution containing 4 mM of H_2PtCl_6 in 0.5 M acid boric. The sputtered gold layer was gently hand polished with 1 μm alumina slurry. After that, the membrane was dissolved in dichloromethane for 30 min to completely release the microtubes. The microrockets were placed on the magnet holding block and the supernatant was removed. Afterwards, successive washes with propan-2-ol and ethanol (both twice) and ultrapure water (18.2 MΩ cm, three times) were performed with 2 min on the magnet holding block between each wash. All microtubes were stored in ultrapure water at room temperature when not in use. The template preparation method resulted in decidedly reproducible micromotors. Template preparation of micromotors is depicted schematically in Figure 5.

Micromotor-based mycotoxin assay

A solution containing 5 μM of the specific fluorophore-labeled aptamer and FB1 or OTA was incubated at 25 °C with gentle stirring for 15 and 60 min for selective recognition, respectively. Then, 5 μL of this mixture containing the aptamer–mycotoxin complex

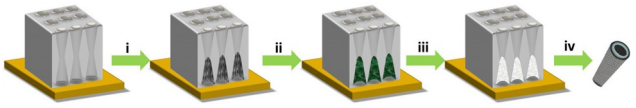

Figure 5. Electrosynthesis of rGO/Ni/PtNPs micromotors. Electrodeposition of outer sensing layer (rGO) (i), intermediate magnetic layer (Ni) (ii), inner catalytic layer (PtNPs) (iii), and micromotors release (iv).

and/or free aptamers was transferred to a microcentrifuge tube containing around 4500 rGO/Ni/PtNPs micromotors, 1 μL of SDS (1% v/v final concentration), and 5 μL of H_2O_2 (1% v/v final concentration). Under these conditions, micromotors were allowed to autonomously swim into the solution to perform on-the-move capture of free aptamers by the outer graphene layer of the micromotors. After 2 min, micromotors were stopped by placing the tube on a magnetic holding block, and three 1 μL aliquots of supernatant were transferred to an inverted optical microscope to record the fluorescence signal. Fluorescence measurements were performed with a B2-A filter ($\lambda_{em}=520$ nm; $\lambda_{ex}=470$ nm) for FB1 and G2-A filter ($\lambda_{em}=602$ nm; $\lambda_{ex}=585$ nm) for OTA. The LOD and LOQ were obtained for $S/N=3$ and $S/N=10$ criteria, respectively. To this end, S was estimated as the fluorescence of the lowest concentration of the calibration graph ($n=10$) and N as the fluorescence in the absence of mycotoxin.

Acknowledgements

This work has been financially supported by the NANOAVANSENS program from the Community of Madrid (S2013/MIT-3029) and the Spanish Ministry of Economy and Competitiveness, CTQ 2014-58643-R (A.E.). A.J. acknowledges the FPI fellowship received from the Spanish Ministry of Economy and Competitiveness (CTQ2011-28153). A.M.-F. acknowledges the FPU fellowship from the Spanish Ministry of Education, Culture and Sports and M.M.-G. acknowledges the NANOAVANSENS program from the Community of Madrid (S2013/MIT-3029) for her postdoctoral contract. Thanks to Dra. San Andrés for her help in the fluorescence characterization. Also, we thank CAI and CNME of Complutense University of Madrid for the Raman and SEM measurements.

Conflict of interest

The authors declare no conflict of interest.

Keywords: adsorption · analytical methods · electrochemistry · micromotors · mycotoxins

[1] M. Guix, C. C. Mayorga-Martinez, A. Merkoçi, *Chem. Rev.* **2014**, *114*, 6285 – 6322.
[2] J. Wang, *Biosens. Bioelectron.* **2016**, *76*, 234 – 242.
[3] H. Wang, M. Pumera, *Chem. Rev.* **2015**, *115*, 8704 – 8735.
[4] J. Katuri, X. Ma, M. M. Stanton, S. Sánchez, *Acc. Chem. Res.* **2017**, *50*, 2 – 11.
[5] J. Li, I. Rozen, J. Wang, *ACS Nano* **2016**, *10*, 5619 – 5634.
[6] S. Sánchez, L. Soler, J. Katuri, *Angew. Chem. Int. Ed.* **2015**, *54*, 1414 – 1444; *Angew. Chem.* **2015**, *127*, 1432 – 1464.
[7] H. Wang, M. Pumera, *Nanoscale* **2017**, *9*, 2109 – 2116.
[8] T. Xu, L. Xu, X. Zhang, *Appl. Mater. Today* **2017**, *9*, 493 – 503.
[9] X. Chen, M. Hoop, F. Musthaq, E. Siringil, C. Hu, B. Nelson, S. Pané, *Applied Materials Today* **2017**, *9*, 37 – 48.
[10] Y. F. Mei, G. S. Huang, A. A. Solovev, E. B. Ureña, I. Mönch, F. Ding, T. Reindl, R. K. Y. Fu, P. K. Chu, O. G. Schmidt, *Adv. Mater.* **2008**, *20*, 4085 – 4090.
[11] A. A. Solovev, Y. F. Mei, E. B. Ureña, G. S. Huang, O. G. Schmidt, *Small* **2009**, *5*, 1688 – 1692.
[12] R. Laocharoensuk, J. Burdick, J. Wang, *ACS Nano* **2008**, *2*, 1069 – 1075.
[13] B. Kherzi, M. Pumera, *Nanoscale* **2016**, *8*, 17415 – 17421.
[14] J. Orozco, B. Jurado-Sánchez, G. Wagner, W. Gao, R. Vazquez-Duhalt, S. Sattayasamitsathit, M. Galarnyk, A. Cortés, D. Saintillan, J. Wang, *Langmuir* **2014**, *30*, 5082 – 5087.
[15] A. Molinero-Fernández, M. Moreno-Guzmán, M. A. López, A. Escarpa, *Anal. Chem.* **2017**, *89*, 10850 – 10857.
[16] J. Wang, *Nanomachines: Fundamentals and Applications*, Wiley-VCH, Weinheim, **2013**.
[17] J. Wang, W. Gao, *ACS Nano* **2012**, *6*, 5745 – 5751.
[18] R. Maria-Hormigos, B. Jurado-Sánchez, A. Escarpa, *Adv. Funct. Mater.* **2017**, 1704256. https://doi.org/10.1002/adfm.201704256.
[19] Y. Mei, A. A. Solovev, S. Sanchez, O. G. Schmidt, *Chem. Soc. Rev.* **2011**, *40*, 2109 – 2119.
[20] W. F. Paxton, K. C. Kistler, C. C. Olmeda, A. Sen, S. K. St. Angelo, Y. Cao, T. E. Mallouk, P. E. Lammert, V. H. Crespi, *J. Am. Chem. Soc.* **2004**, *126*, 13424 – 13431.
[21] W. Gao, S. Sattayasamitsathit, J. Orozco, J. Wang, *J. Am. Chem. Soc.* **2011**, *133*, 11862 – 11864.
[22] G. Zhao, M. Pumera, *RSC Adv.* **2013**, *3*, 3963 – 3966.
[23] A. Martín, B. Jurado-Sanchez, A. Escarpa, J. Wang, *Small* **2015**, *11*, 3568 – 3574.
[24] R. Maria-Hormigos, B. Jurado-Sanchez, L. Vazquez, A. Escarpa, *Chem. Mater.* **2016**, *28*, 8962 – 8970.
[25] D. Vilela, J. Parmar, Y. Zeng, Y. Zhao, S. Sanchez, *Nano Lett.* **2016**, *16*, 2860 – 2866.
[26] H. Cheng, C. Hu, Y. Zhao, L. Qu, *NPG Asia Mater.* **2014**, *6*, 113.
[27] B. Esteban-Fernández de Ávila, M. A. Lopez-Ramirez, D. F. Baez, A. Jodra, V. V. Singh, K. Kaufmann, J. Wang, *ACS Sens.* **2016**, *1*, 217 – 221.
[28] Y. Shao, J. Wang, M. Engelhard, C. Wang, Y. Lin, *J. Mater. Chem.* **2010**, *20*, 743 – 748.
[29] E. Morales-Narváez, A. Merkoçi, *Adv. Mater.* **2012**, *24*, 3298 – 3308.
[30] N. S. Green, M. L. Norton, *Anal. Chim. Acta* **2015**, *853*, 127 – 142.
[31] C. H. Lu, H. H. Yang, C. L. Zhu, X. Chen, G. N. Chen, *Angew. Chem. Int. Ed.* **2009**, *48*, 4785 – 4787; *Angew. Chem.* **2009**, *121*, 4879 – 4881.
[32] B. Pérez-López, A. Merkoçi, *Microchim. Acta* **2012**, *179*, 1 – 16.
[33] H. P. Van Egmond, R. C. Schothorst, M. A. Jonker, *Anal. Bioanal. Chem.* **2007**, *389*, 147 – 157.
[34] EC. No. 123 – 2005, EC. No.1881 – 2006, Commission Regulation No. 1126/ 2007, European Commission, 2007.
[35] N. W. Turnera, S. Subrahmanyamb, S. A. Piletskyb, *Anal. Chim. Acta* **2009**, *632*, 168 – 180.
[36] A. Jodra, M. A. López, A. Escarpa, *Biosens. Bioelectron.* **2015**, *64*, 633 – 638.
[37] A. Jodra, M. Hervás, M. A. López, A. Escarpa, *Sens. Actuators B* **2015**, *221*, 777 – 783.
[38] A. H. Loo, A. Bonanni, M. Pumera, *ChemElectroChem* **2015**, *2*, 743 – 747.
[39] F. Berthiller, C. Brera, C. Crews, M. H. Iha, R. Krska, V. M. T. Lattanzio, S. MacDonald, R. J. Malone, C. Maragos, M. Solfrizzo, J. Stroka, T. B. Whitaker, *World Mycotoxin J.* **2016**, *9*, 5 – 29.
[40] S. Wu, N. Duan, X. Ma, Y. Xia, H. Wang, Z. Wang, Q. Zhang, *Anal. Chem.* **2012**, *84*, 6263 – 6270.
[41] R. María-Hormigos, B. Jurado-Sánchez, A. Escarpa, *Nanoscale* **2017**, *9*, 6286 – 6290.

Manuscript received: December 22, 2017
Accepted manuscript online: February 22, 2018
Version of record online: April 16, 2018

